Er^{3+} Concentration Effects in Commercial Erbium-Doped Silica Fibers Fabricated Through the MCVD and DND Technologies

Alexander V. Kir'yanov, *Member, IEEE*, Yuri O. Barmenkov, *Member, IEEE*, Gabriel Eduardo Sandoval-Romero, and Luis Escalante-Zarate

***Abstract*— Commercial Erbium doped silica fibers fabricated through the modified chemical vapor deposition and direct nanoparticle deposition processes where Er^{3+} concentration is varied in a wide range are characterized by means of analyses of Er^{3+} fluorescence decay kinetics and nonlinear absorption coefficient at 978-nm pumping. Through theoretical modeling of the results of the entire experiment, the values of key parameters for the concentration-related effects, i.e. homogeneous and inhomogeneous upconversion processes, are determined.**

***Index Terms*— Erbium-doped silica fibers, homogeneous and inhomogeneous upconversion, Er^{3+} concentration, MCVD and DND technologies, modeling.**

I. Introduction

OPTICAL engineering with Erbium doped silica fibers (EDFs) became in the past two decades enormously extensive, given by the expanding needs of such telecom oriented devices as EDF based lasers and amplifiers. In the meantime, interest to EDFs has immanent reasons as to objects for basic studies.

One of the points that attracted attention of the fiber community from 1990-ies [1]–[15] throughout 2000-ies [16]–[30] till nowadays [31]–[34] is Er^{3+} concentration effects in EDFs. During the period the theme was visited by a number of research groups with an aim to clear up the laser/ amplifying potential of EDFs heavily-doped with Er^{3+} where these effects are presumably deteriorating. As the result of the studies, the main drawbacks have been clearly revealed, which accompany an increase of Er^{3+} content in EDFs, such as $\sim$1.5-μm fluorescence quenching, caused by homogeneous upconversion (HUC), and reduced efficiency of EDF based lasers and amplifiers, associated with the phenomenon of Er^{3+} ions' clustering and resulted in growth of non-saturable absorption (NSA) through inhomogeneous upconversion (IUC).

Another, mostly negative, effect stemming from intrinsic multi-level energy structure of the Er^{3+} ion, the excited state absorption (ESA) in EDFs, was also under scope during the past years; see *e.g.* Refs. [35]–[42]. Definitive but hidden on the first glance inter-connection of the aforementioned concentration effects (fluorescence quenching and NSA) with the ESA phenomenon deserves noticing.

Despite of general understanding of the matter, there still exist certain gaps concerning certain aspects of the concentration-related HUC / IUC phenomena in EDFs and the parameters featuring them. As far as we know there was no any research towards characterization of Er^{3+} concentration effects in commercial EDFs. Sometimes a lack of the data on Er^{3+} concentration effects in such fibers leads to confusions at their usage.

The most known representatives of commercial EDFs at the fiber market are so-called "M" and "L" fibers, fabricated through the modified chemical vapor deposition (MCVD) and direct nanoparticle deposition (DND) processes. The EDFs of these two types are similar in the sense of chemical composition of Er^{3+} doped core (the most common alumino-silicate glass, in case of M EDFs with addition of germanium), thus being worthy of a comparison. The present work was fulfilled for two types of M fibers (*Fibercore* M5-125-980 and M12-125-980, hereafter M5 and M12) and three types of L-fibers (*Leikki/nLight* L20-4/125, L40-4/125, and L110-4/125, hereafter L20, L40 and L110). As seen from Table 1, the EDFs of L series are somewhat a "continuation" of the ones of M series in the aspect of Er^{3+} concentration increase.

The main motivation of the present work was a straightforward characterization of the EDFs of L and M types in attempt of developing simple but reliable measurement and modeling routes to attest them in terms of the Er^{3+} concentration-related phenomena. We study these fibers by means of analyses of Er^{3+} fluorescence decay kinetics and nonlinear absorption coefficient at 978-nm pumping, strongly affected by the HUC and IUC effects.

We believe that the obtained data would impact upon further research activity and commercial usage of these or similar EDFs.

II. Experimental

A. Absorption and Fluorescence Spectra

The EDFs' absorption spectra are shown in Fig. 1 where Er^{3+} transitions $^4I_{15/2} \rightarrow {}^4I_{11/2}$ (within a 940–1030 nm range with a peak at 978 nm) and $^4I_{15/2} \rightarrow {}^4I_{13/2}$ (within a 1400–1600 nm range with a peak at 1.53 μm) are featured.

Manuscript received November 15, 2012; revised March 7, 2013; accepted March 28, 2013. Date of publication April 15, 2013; date of current version May 1, 2013. This work was supported in part by the UNAM-DGAPA (PAPIIT-IT101712).

A. V. Kir'yanov is with the Centro de Investigaciones en Optica, Leon 37150, México (e-mail: kiryanov@cio.mx).

Y. O. Barmenkov and L. Escalante-Zarate are with the Centro de Investigaciones en Optica, Leon 37150, México (e-mail: yuri@cio.mx; itrio@cio.mx).

G. E. Sandoval-Romero is with the Centro de Ciencias Aplicadas y Desarrollo Tecnológico, Universidad Nacional Autónoma de México, México D. F. 04510, México (e-mail: eduardo.sandoval@ccadet.unam.mx).

Digital Object Identifier 10.1109/JQE.2013.2257691

TABLE I

BASIC PROPERTIES OF THE EDFS OF L AND M TYPE (6 LEFT COLUMNS) AND Er^{3+} CONCENTRATION-RELATED PARAMETERS OBTAINED FROM THE CURRENT EXPERIMENTS AND MODELING (4 RIGHT COLUMNS)

EDF	Small-Signal Absorption @978 nm α_0 [dB/m]	Core Radius r_0 [μm]	NA	Overlap Factor Γ	Mode Field Radius @978 nm r_m [μm]	Erbium Concentration N_0 [cm^{-3}] $\times 10^{18}$ [Estimate]	Nonsaturable Absorption @978 nm β [dB/m] [Estimate at ~400 mW]	Er^{3+} Clusters Contribution κ [%] [at $\Omega = 2$]	Fluorescence Decay τ_0 [ms]	HUC Parameter C_{HUP} [s^{-1}]
M5	5.0	1.5	0.23	0.77	1.75	8.8	0.4 ± 0.1	3.6 ± 0.7	10.8 ± 0.3	11 ± 5
M12	12.5	1.5	0.23	0.77	1.75	21.1	1.5 ± 0.2	7.7 ± 0.9	10.8 ± 0.3	30 ± 5
L20	12.0	1.8	0.20	0.80	2.04	20.3	1.7 ± 0.2	6.9 ± 0.8	10.8 ± 0.3	30 ± 5
L40	23.0	1.8	0.20	0.80	2.04	38.9	4.1 ± 0.4	10.8 ± 1.1	10.8 ± 0.3	58 ± 5
L110	67.5	1.8	0.20	0.80	2.04	113.5	15.5 ± 0.9	18.7 ± 1.6	10.8 ± 0.3	168 ± 5

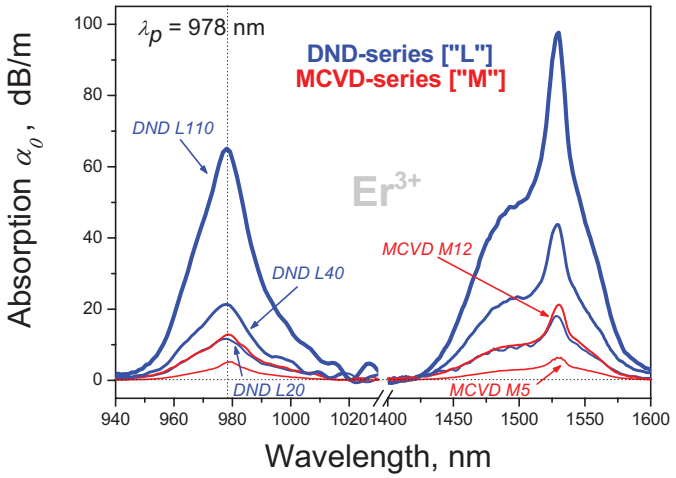

Fig. 1. Absorption spectra of the EDFs of L (blue curves) and M (red curves) series in near-IR.

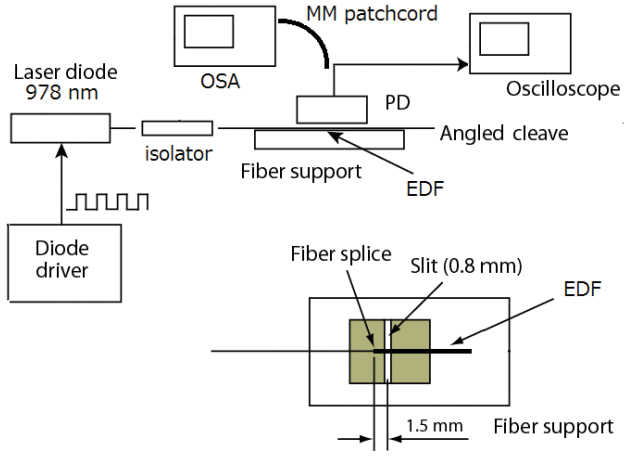

Fig. 2. Experimental arrangement for measurements of fluorescence spectra/fluorescence kinetics of the EDFs.

Hereafter the EDF samples are labeled in accordance to the fabricants' notations, given by the fibers' small-signal absorption (SSA) coefficients α_0 [in dB/m] at ~1.53 μm (L series) and 978 nm (M series), respectively. The spectra were obtained using a white light source with fiber output and an optical spectrum analyzer (OSA). The EDFs' off-resonance attenuations (at ~1.3 μm) were measured to be two orders of magnitude lower than absorptions in the peaks of the Er^{3+} bands. It is seen that, in contrast to the results of Ref. [13], the absorption spectra of the EDFs of both series have a very similar shape (given by similarity of core glass chemical compositions), differing only in intensity. The ratio of the peaks' magnitudes at 1.53 μm and at 978 nm was measured to be also equal (~1.6) for the EDFs of both M and L series.

The EDFs' fluorescence spectra were measured in lateral geometry at in-core pumping. Figure 2 sketches the setup we used at the measurements of Er^{3+} fluorescence spectra and, as it follows, Er^{3+} fluorescence kinetics.

The pump wavelength $\lambda_P = 978$ nm is seen (Fig. 1) to coincide with the ground-state absorption (GSA) transition of the Er^{3+} ion ($^4I_{15/2} \rightarrow {}^4I_{11/2}$). We used for pumping a standard laser diode (LD) with fiber output in conjunction with a fiber isolator for 980 nm, protecting LD against parasitic back reflections; the isolator's output fiber was spliced with EDF samples.

In the experiments, we used short (~0.5 cm) pieces of EDFs for minimizing influence of amplified spontaneous emission (ASE), reabsorption, and gain, which are expected to be pronounced especially in the fibers with the highest Er^{3+} content. Fluorescence was collected from the lateral surface of a fiber sample (at the point located ~1.5 mm away from the splice with the isolator fiber), using a multimode patchcord connected to the OSA; see Fig. 2.

Figure 3 exemplifies the normalized fluorescence spectra for L fibers, measured at maximal pump power P ~400 mW within the 450…1650 spectral range (the area nearby the pump wavelength was cut out from the spectra).

It is seen that the Er^{3+} fluorescence band, centered at ~1.53 μm (transition $^4I_{13/2} \rightarrow {}^4I_{15/2}$), is indistinguishable in shape in the row of fibers L20→L40→L110, where Er^{3+} concentration increases. Furthermore, the normalized integrated powers within the 1.53-μm band reveal (see inset to Fig. 3) vastly equal saturation character of fluorescence at increasing pump power, which stems from saturating of population of Er^{3+} $^4I_{13/2}$ manifold where the fluorescence originates from. The saturating pump power is estimated by ~2 mW, a characteristic value for EDFs of such type; see *e.g.* [31]).

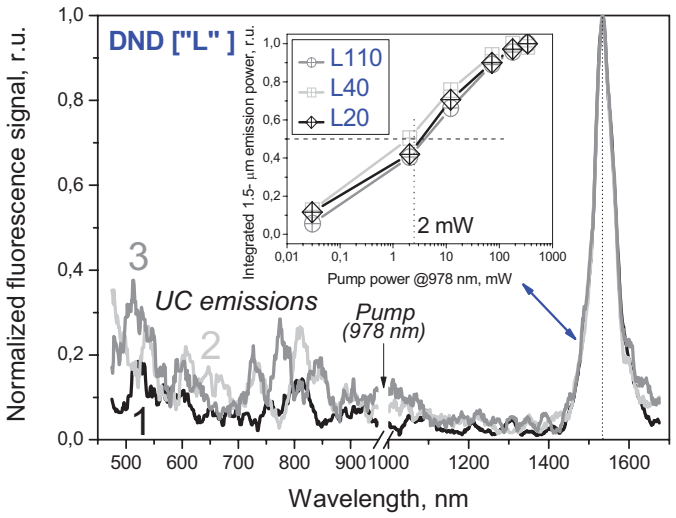

Fig. 3. Fluorescence spectra of the EDFs of L type in VIS-to-near-IR spectral range at 978 nm pumping: L20 (curve 1); L40 (curve 2); L110 (curve 3). Inset shows the dependences of integrated (1400–1650 nm) fluorescence power *vs.* pump power.

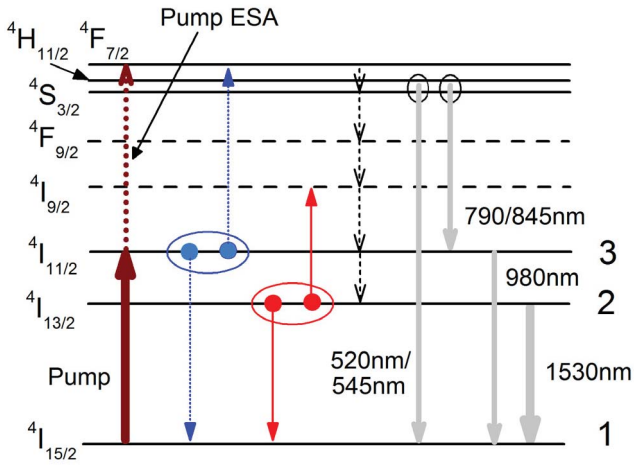

Fig. 4. Scheme of energy levels of Er^{3+}, applicable for the EDFs with high Er^{3+} content. Functioning of Er^{3+} clusters (shown for simplicity as ion pairs) is sketched by the blue and red arrows for manifolds $^4I_{11/2}$ and $^4I_{13/2}$; the black dotted arrows depict non-radiative relaxations while the grey ones show UC and "fundamental" 1.53-μm emissions. The short-living levels are shown by dashed lines.

Although the 1.53-μm band dominates in the EDFs' fluorescence spectra, there also exist the spectral lines at its anti-Stokes side (~450…1100 nm), which evidences the presence of upconversion (UC) processes in the fibers. Note that, in contrast to the 1.53-μm band's stability against Er^{3+} concentration, the higher Er^{3+} concentration the more intense are the UC emissions (compare curves 1 – 3 in Fig. 3).

The concentration dependence of UC emissions for the EDFs of L and M types, integrated over the spectral interval 450–1100 nm and normalized on the integrated "fundamental" (1400–1650 nm) emission, is shown by curve 2 in Fig. 8 (to be discussed in more detail below). Most probably, this trend is associated with growth of percentage of clustered Er^{3+} ions in the EDFs at increasing Er^{3+} concentration.

To understand the origin of the UC emissions and the dependence of UC intensity upon Er^{3+} concentration in the EDFs, the reader is advised to refer to Fig. 4 where we present the scheme of Er^{3+} energy levels and sketch the processes involved at the excitation at $\lambda_P = 978$ nm. The UC emissions (shown in the figure by grey thin arrows) seems to be mostly associated to Er^{3+} ion clusters being in the states $^4I_{11/2}$ and $^4I_{13/2}$, because the ESA process, equally acting for single and clustered Er^{3+} ions, is quite ineffective at 978-nm excitation.

B. Fluorescence Decay Kinetics

The kinetics of near-IR fluorescence at ~1.53 μm was measured by employing the same arrangement ("lateral geometry") as at the measurements of fluorescence spectra (see Fig. 2). However, the pump light at 978 nm was in this case switched on / off by applying a rectangular modulation of LD current at Hz-repetition rate. The launched into the EDF samples pump power P_{978} was varied between zero and ~400 mW. The fluorescence signal was detected either using an InGaAs photo-detector (PD) with a Si filter placed in between the fiber and a multimode patchcord delivering fluorescence to PD (the use of Si filter allowed us to cut off the pump light's spectral component), or using a fast Si-PD (without any spectral filtering) placed directly above a slit segregating a portion of fluorescence leaving the EDF's surface; see Fig. 2. Likewise at the measurements of fluorescence spectra, we used very short pieces of the EDFs (~0.5 cm) for ensuring negligible effect of ASE and reabsorption on the results. Both the detectors had approximately plain response within the characteristic spectral intervals: 800–2200 (InGaAs-PD, time resolution of ~1.6 μs) and 400–1070 (Si-PD, time resolution of ~0.8 μs). The overall setup's time resolution has been checked prior to the main-course experiments using a standard Er^{3+} -free fiber; it was found to be 8±1 μs (a common value; see *e.g.* [24]), given mainly by the LD driver's temporal response.

Typical kinetics of the fluorescence signal, recorded after switching off pump light, are presented in Fig. 5 for the heavier doped EDFs L110 (a) and M12 (b); the data were acquired using InGaAs-PD with Si filtering. [We don't present here results for other, lower doped, EDFs as these show similar but less featured trends in the decay kinetics].

It is seen from Fig. 5 that for the two EDFs fluorescence power corresponding to 1.53-μm spectral band is saturated (as is saturated GSA of Er^{3+} ions) yet at a few mW of pump power: compare with inset to Fig. 3. However the key feature seen in Fig. 5(a) is deviation from the exponential law in the fluorescence kinetics in EDF L110. Notice that a similar trend occurs but is less noticeable in the rest of L and M fibers with lower Er^{3+} concentration; see *e.g.* Fig. 5(b). Another fact deserving attention is the presence of a sharp drop in the fluorescence signal in fiber L110 at high pump powers, which happens after switching pump off (refer to curves 4–6 in Fig. 5(a)). Such a drop is also present but in a lesser degree in fibers L40, L20, and M12 (having substantially lower Er^{3+} contents) and almost vanishes in fiber M5 (having the lowest Er^{3+} content). Note that similar fluorescence

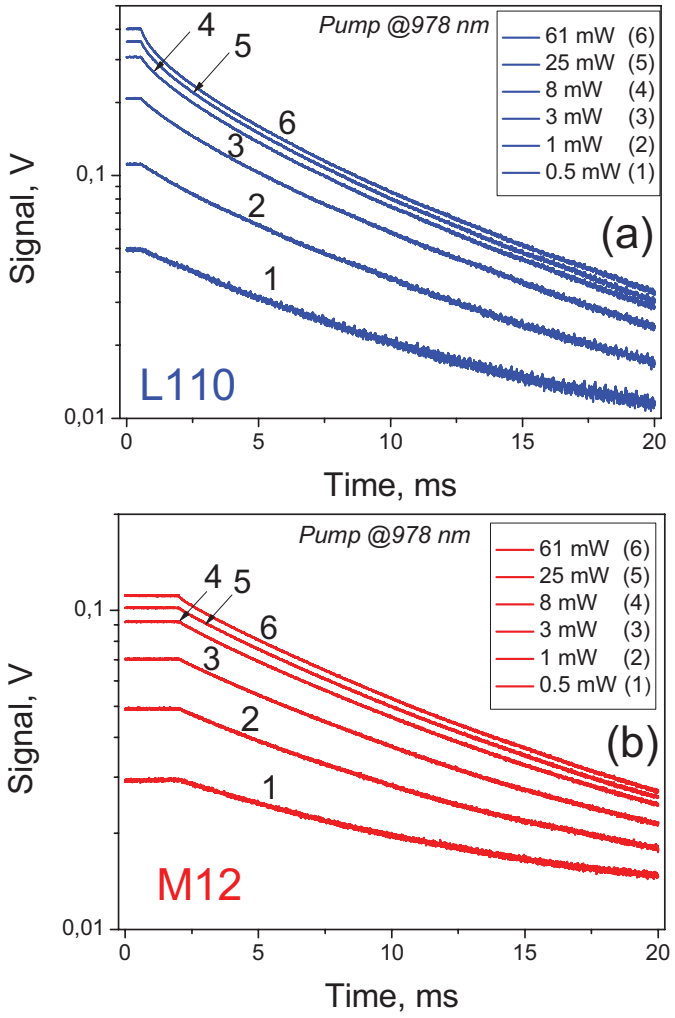

Fig. 5. Fluorescence decay kinetics obtained for the EDFs L110 (a) and M12 (b) using InGaAs-PD with Si filtering. Curves 1 to 6 correspond to increased pump powers (see insets).

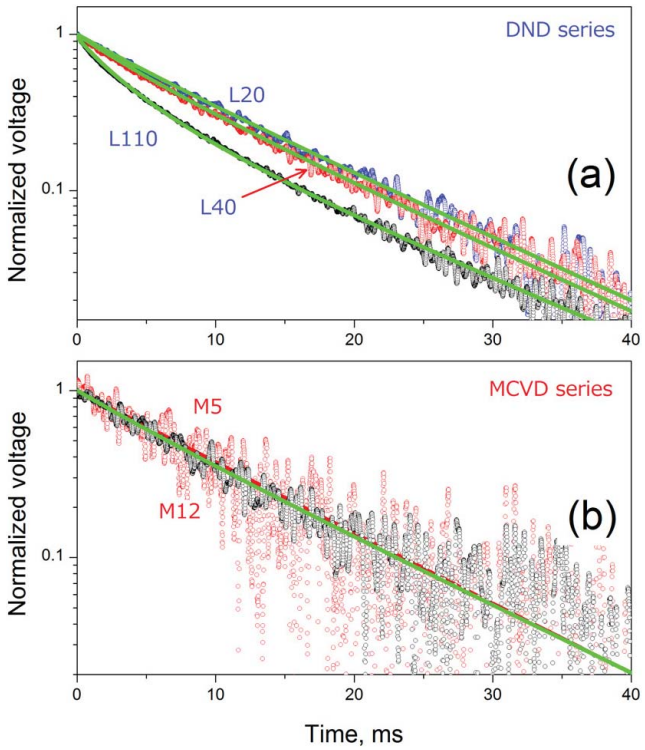

Fig. 6. Normalized fluorescence decay kinetics obtained for the EDFs of L (a) and M (b) series; points – experimental data (using InGaAs-PD with Si filtering); plain curves – theoretical fits made employing formula (2).

kinetics were observed in some of the earlier reports, see *e.g.* Refs. [3], [36].

Overview of the fluorescence decays for the whole of the EDFs is provided in Fig. 6 (points). These data were obtained using the same experimental arrangement at P_{978} ~400 mW; the high pump power was found to be the right choice for minimizing spatial diffusion of excitation (see *e.g.* Ref. [3]) and for making a proper modeling as it is explained below in Section III.A. Notice that the dependences shown in Fig. 6 are the fluorescence decay tails obtained after cutting off the short temporal segments measured by ~30 μs, corresponding to the above mentioned sharp drop in the fluorescence signal (see Fig. 5); there are also subtracted in Fig. 6 the PD offsets, presented in the original experimental data.

It is seen from Fig. 6 that 1.53-μm fluorescence decays get more and more deviated from the single exponential law when Er^{3+} concentration increases. Namely, the fibers with smaller contents of Er^{3+} ions (M5, M12, and L20) demonstrate decays very close to the single-exponent law whereas fibers L40 and L110 are characterized by decays, apparently not obeying this law.

The revealed features, associated to the Er^{3+} concentration effect, can be addressed in terms of the HUC process – see Section III where the results of modeling of Er^{3+} fluorescence kinetics are presented. The modeling of fluorescence decay allowed us to get, for each EDF, lifetime τ_0 and HUC constant C_{HUP}* and to build thereafter their dependences against the SSA value α_0 (and hereby against Er^{3+} ions concentration, proportional to α_0).

Figure 7 demonstrates the results of the fluorescence kinetics measurements within a short (tens of μs) interval just after switching pump light off, for the EDFs L20 (a), L40 (b), L110 (c) and, for comparison, M12 (d). The measurements were fulfilled using Si-PD without optical filtering at P_{978} ~400 mW.

It is seen from Fig. 7(b–d) that, in the presence in the PD's response of the shortest component measured by ~8 μs (the setup's technical resolution; see above), originated from the scattered pump light, there also exist the short components measured by 21±2 μs and 23±2 μs for fibers L110 and L40 and 26±2 μs for fiber M12 (for fibers L20 and M5 this component was not resolved). Remind that the same component was detected in the 1.53-μm fluorescence kinetics; see Fig. 5, thus pointing out its non-radiative character. Interestingly, there are known other processes in Erbium-doped materials attributed by similar times; see *e.g.* Refs. [43], [44].

We propose that the found feature is an attribute of partial relaxation of excitation in Er^{3+} clusters since it is presented in the heavier doped EDFs but almost vanishes in the lower doped ones. The magnitude of the short-living component was

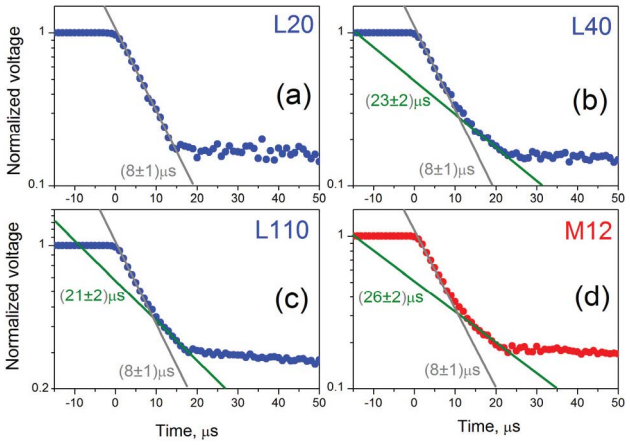

Fig. 7. Fluorescence decay kinetics in the EDFs measured using Si-PD: L20 (a), L40 (b), L110 (c), and M12 (d); the technical resolution and the short-time components of the fluorescence signals are specified in each plot. The zero times correspond to the moments of switching LD driver's current off.

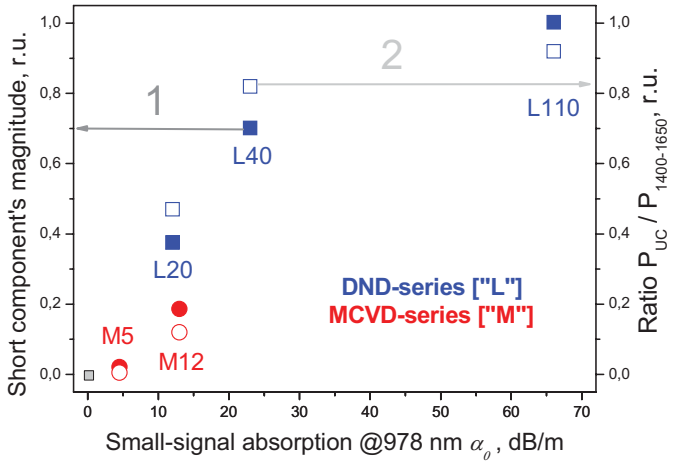

Fig. 8. Magnitude of the short-living component in fluorescence decays (curve 1) and the ratio between the integrated powers P_{UC} (in UC fluorescence region, 450–1000 nm) and $P_{1400-1650}$ ("fundamental" emission, 1400–1650 nm) (curve 2) *vs.* Er^{3+} concentration in terms of SSA α_0, obtained for the EDFs of L and M types.

found to be a function of Er^{3+} concentration (and α_0), as apparent when comparing plots (a), (b), and (c) in Fig. 7 for the EDFs of L series: The higher Er^{3+} concentration the larger its relative – to the pump-light scattering component – magnitude.

It deserves mentioning the following: In fact, what is detected by the Si-PD in the last experiments is the UC fluorescence, spectrally limited to the interval ~450…1100 nm (refer to Fig. 3). As it was revealed at discussion of the data shown in Fig. 3, overall UC power grows with increasing Er^{3+} content in the fibers; see empty symbols (curve 2) in Fig. 8. In order to shed more light on the physics behind this, we demonstrate in the same figure the relative magnitude of the short-living component as a function of the SSA value for the whole EDFs set (see filled symbols, curve 1). This dependence also clearly demonstrates the Er^{3+} concentration effect in terms of SSA α_0. Thus, the short-living (~20…30 μs) component detected for the EDFs heavier doped with Er^{3+} seems to be related to excitation relaxation in Er^{3+} clusters, thus being apparently a side of the IUC process. As it is argued in the following Section III, the presence of this concentration-dependent, μs-range, mostly non-radiative relaxation can be ascribed to the presence in the EDFs of "quenched" Er^{3+} ion clusters.

C. Nonlinear Absorption Coefficient

The nonlinear absorption coefficient of a rare-earth doped fiber as a function of pump power $\alpha(P)$ contains the useful information about GSA saturation and thereafter about the fiber's potential as a laser medium. On the other hand, such effects deteriorating laser "quality" of an EDF as ESA and concentration-related HUC / IUC (lifetime quenching and NSA) ought to contribute in the behavior of $\alpha(P)$, too [21].

We inspected the dependences $\alpha(P)$ for the EDFs at CW pumping at $\lambda_e = 978$ nm, the most relevant experimental arrangement.

Pump light was delivered to an EDF sample from the same LD used at the measurements of fluorescence spectra and lifetimes; pump power launched into the fiber, P^{in}, was varied from ~0.5 to ~400 mW. A tested fiber was spliced to the output fiber of the same isolator, connected to the LD output fiber. First, we measured (using a standard power meter) the nonlinear transmission coefficient of the EDF sample with length L_0, which is defined as $T_{978} = P^{out}/P^{in}$, where P^{in} and P^{out} are the pump powers at the EDF input and output. Then we made a formal re-calculation of the experimental transmission coefficient $T_{978}(P^{in})$ into the absorption coefficient, applying formula: $\alpha(P^{in}) = -ln(T_{978})/L_0$.

Notice that the EDFs' lengths (see caption to Fig. 9) were chosen such that overall trends in the dependences $\alpha(P^{in})$ within the whole range of pump powers can be viewed. At the same time, the ratio of the EDFs' lengths was such that optical density (the product $\alpha_0 L_0$) be almost the same for either EDF sample – for seeing the NSA effect at increasing Er^{3+} concentration (SSA α_0) in the fibers. Using the OSA, we checked the ratio of pump to ASE powers at the EDFs outputs; the ASE contribution was found to be negligible for all the fibers at $P^{in} > 0.5$ mW.

The results obtained by applying the drawn procedure are shown in Fig. 9 by symbols. As usually the data for the fibers of M (M5 and M12) and L (L20, L40, and L110) series are highlighted by red (curves 1 and 2) and blue (curves 3 to 5) colors. Coefficients α_0 and β marked in the upper left and right corners of the figure correspond to the limits of small-signal and pump-saturated absorptions.

When examining the experimental data plotted in Fig. 9, the nonlinear character of the dependences $\alpha(P^{in})$ becomes apparent.

First notice that absorption is "bleached" (in other words, transmission is "saturated") by a more or less similar manner for either fiber. However, as it is also seen from the figure, the residual absorption (coefficient β) rises drastically with increasing Er^{3+} concentration in the fibers' sequences M5→M12 and L20→L40→L110). This trend points out that the ratio between the residual (β) and small-signal (α_0)

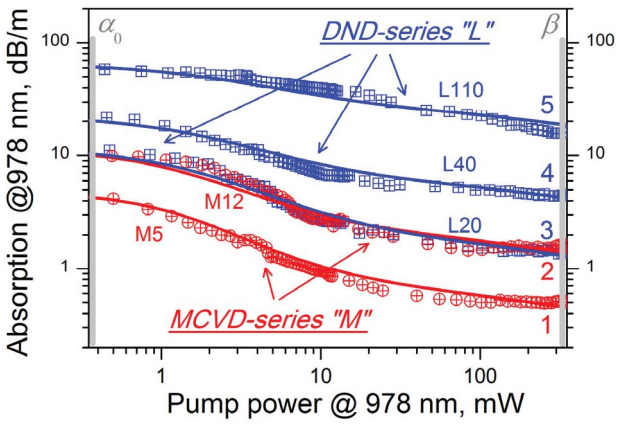

Fig. 9. Nonlinear absorption coefficients of EDFs of L and M types *vs.* pump power at 978 nm: symbols – experimental data; plain curves – theoretical fits obtained using Eqs (4–6). Fiber lengths used in experiments and at modeling were, correspondingly: 188.6 (M5, curve 1), 59.4 (M12, curve 2), 43.5 (L20, curve 3), 22.4 (L40, curve 4), and 9.5 (L110, curve 5) cm.

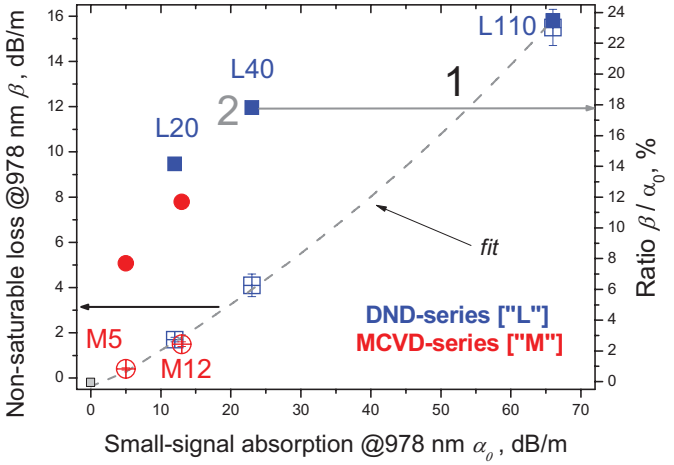

Fig. 10. Non-saturable absorption β (curve 1) and ratio β/α_0 (curve 2) *vs.* Er^{3+} concentration in terms of SSA α_0, measured for the entire set of EDFs of L and M types; the fitting curves are for guiding the eye.

absorptions is much bigger for the heavier doped fibers (M12, L40 and L110). In fact, pump-induced absorption β is the measure of NSA loss in an EDF. Indeed, the dependence β (α_0) plotted in Fig. 10 by curve 1 (crossed symbols) shows the excessive (NSA) loss in the EDFs as the appearance of Er^{3+} concentration effect.

Interestingly, growth of ratio β/α_0 *vs.* SSA-value α_0 (shown by curve 2 in Fig. 10) demonstrate analogy to the trends that have the short-time component in the Er^{3+} fluorescence kinetics and the UC emission power *vs.* α_0 – refer to curves 1 and 2 in Fig. 8. Thus, we can propose that all these quantities have a common cause, the fast relaxation of excitation within the subsystem of Er^{3+} clusters via IUC.

Resuming the experimental results shown in Figs. 8–10, let's emphasize that the nonlinear character of the EDFs' absorption coefficient *vs.* pump power at 978 nm is mostly defined by the contributions stemming from the Er^{3+} GSA saturation (a usual effect for any EDF) and from the IUC process (a much severe effect in EDFs heavily doped with Er^{3+}).

III. Modeling

Here we develop a model that allows understanding and simple interpreting of the experimental results reported in Section II, *i.e.* the kinetics of near-IR fluorescence (Figs. 5 and 6) and the nonlinear absorption coefficient (Figs. 9 and 10) of the EDFs. In the model, we account for the GSA / ESA transitions interplay and Er^{3+} concentration-related effects (the HUC and IUC processes). By fitting the modeling results to the experimental data, we find the values of some important parameters, useful for applications. Notice that the present model is based on the approach, developed by us earlier [45] for addressing nonlinear-optical properties of Bismuth-doped silica fibers.

A. Fluorescence Decay

First we model the kinetics of near-IR (~1.53 μm) fluorescence decays obtained for the entire set of the EDF samples (M and L). This allows us to find fluorescence lifetimes τ_0 and HUC coefficient C_{HUP}. As a preface, notice that our model implicitly implies, accordingly to the definition of the HUC process, interactions only between rather distant *single* Er^{3+} ions, not forming "chemical", tightly coupled, *clusters*, which are in turn supposed to interact via the IUC mechanism to be modeled further (subsection III.B). In other words, at this step of modeling we disregard the short-time features in fluorescence decays reported in Fig. 7, which are assumed to originate from Er^{3+} ions gathered into quenched (weakly fluorescing) clusters. That fact that in the experiments on fluorescence kinetics we used comparatively high pump powers (P_{978} ~400 mW) allows us to neglect further an intensity-dependent HUC contribution and the excitation migration effects.

As it is seen from Figs. 5 and 6, once concentration of Er^{3+} ions (and thus SSA) increases the ~1.53-μm fluorescence decay kinetics gets more and more deviated from the single-exponent law. For EDFs, such behavior definitely stems from HUC, *i.e.* from energy transfer between two equivalent single centers, both being in the excited state 2 ($^4I_{13/2}$), with the result that one of them transits to the ground state 1 ($^4I_{15/2}$) and another one, after upstairs transition (ESA) to the higher lying state 3 $^4I_{9/2}$ and subsequent fast non-radiative relaxation, remains in the excited state 1; see Fig. 4. It is clear that this should inevitably result in a non-exponential character of the decay kinetics, usually referred to as fluorescence quenching.

For the normalized population density n_2^S of single (index "*s*") Er^{3+} ions being in the first excited state $^4I_{13/2}$, the following rate equation holds:

$$\frac{dn_2^S}{dt} = -\frac{n_2^S}{\tau_0} - C_{HUP}\left(n_2^S\right)^2 \tag{1}$$

where $n_2^S = N_2^S/N_0^S$; N_2^S is the population density of single Er^{3+} ions in the excited state 2 ($^4I_{13/2}$), N_0^S is their concentration, and C_{HUP} [s^{-1}] is the UC parameter, being a product of the "volumetric" HUC constant C_{HUP}* [$s^{-1}cm^3$] and concentration N_0^S: $C_{HUP} = N_0^S C_{HUP}^*$.

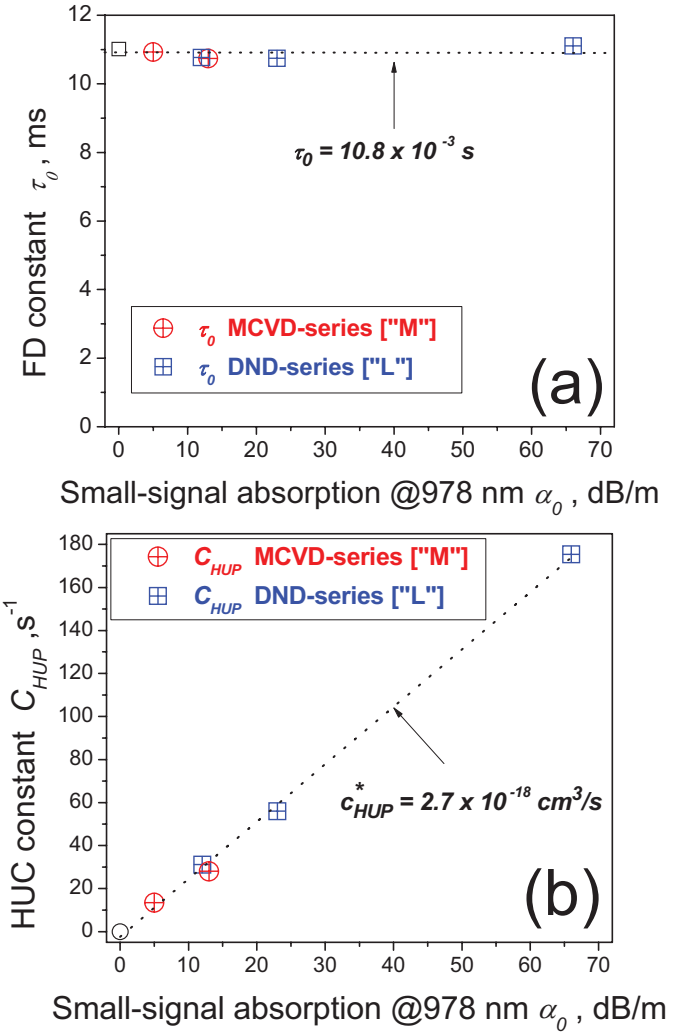

Fig. 11. The values of fluorescence decay constant τ_0 (a) and HUC constant C_{HUP} (b) *vs.* Er^{3+} concentration (in terms of SSA α_0), obtained for the entire set of EDFs of L and M types as the result of modeling the experimental fluorescence kinetics; the fitting curves are for guiding the eye.

We assume further that pump power at 978 nm is high enough to achieve maximal populating of the excited state 1 (it is limited from above by the relation between the GSA and stimulated emission (SE) cross-sections, σ_{12} and σ_{21}). At this assumption, *i.e.* at "infinite" pump power, the part of Er^{3+} ions being in the excited state is $k = \sigma_{12}/(\sigma_{12} + \sigma_{21})$. Furthermore, in our experimental circumstances (where near-IR fluorescence is detected at ~1.53 μm while excitation is at $\lambda_P = 978$ nm) the SE process can be disregarded by means of formal zeroing cross-section σ_{21} in dominator of this ratio: $k = 1$. Then, implying that $n_2^s(t = 0) \equiv 1$ and that pump is switched off at $t = 0$, Eq. (1) is solved analytically:

$$n_2^S(t) = \frac{e^{-\frac{t}{\tau_0}}}{1 + \tau_0 C_{HUP}\left(1 - e^{-\frac{t}{\tau_0}}\right)}. \qquad (2)$$

Formula (2) is a worthy approximation for fitting the whole of experimental near-IR fluorescence decay kinetics reported in subsection II.B for P_{978} ~400 mW, provided by maximal populating of manifold $^4I_{13/2}$ (see Fig. 6). The modeling results obtained by employing formula (2) are shown by plain curves in Fig. 6 (the fitting procedure has been fulfilled until the residual sum R^2 exceeded 0.99) and are in good agreement with the experimental decay kinetics (points in the figure). The values of constants τ_0 (lifetime of single Er^{3+} ions) and C_{HUP} (an attribute of HUC), which have been determined as the result of fitting are plotted in Fig. 11 in function of the SSA value α_0.

It is seen that ~1.53-μm fluorescence lifetime is 10.8±0.3 ms for the fibers of both types, being almost independent of Er^{3+} concentration (the SSA value); see Fig. 11(a). Notice that this value is consistent with the data provided by the manufacturers of the fibers. In contrast, parameter C_{HUP} is expected to be proportional to Er^{3+} concentration (SSA α_0), which allows us to get the value of HUC constant: $C_{HUP}{}^* = 2.7\times10^{-18}$ $s^{-1}cm^3$; see Fig. 11(b). This value agrees well with the published data for EDFs of similar types; see *e.g.* Refs. [32]–[34].

As far as we know, no data regarding the HUC phenomenon in the commercial EDFs of M and L types are available; in this sense the found $C_{HUP}{}^*$ constant would be useful for practice with these EDFs.

Notice that the quantity addressing the HUC phenomenon ($C_{HUP}{}^*$ constant) should be proportional to the ESA cross-section (see *e.g.* Ref. [11]). As the latter does not depend on Er^{3+} concentration, $C_{HUP}{}^*$ should be in the first approximation concentration-independent. Indeed, the dependence C_{HUP} on α_0 is seen from Fig. 11(b) to be almost linear.

B. Nonlinear Absorption Coefficient

A method to model nonlinear absorption of an EDF is based on the idea that ensemble of Er^{3+} ions in a fiber consists of two independent subsystems, assumed to be single ("*s*") and clustered ("*c*") ions. Considering this hypothesis, we generalize the model developed in Ref. [45] for propagation of a pump wave through the system of single and paired resonantly absorbing and fluorescing centers (pairs are the simplest case of clusters). The model's generalization signifies here that the clusters' subsystem is meant to comprise an arbitrary number of centers (Er^{3+} ions in our case) whereas the other subsystem – to consist of single species [2], [10].

We reduce the complex level system of Er^{3+} ions (refer to Fig. 4) to the simplified one composed of three equivalent levels, with level 1 being the ground state ($^4I_{15/2}$), level 2 the first excited state (effectively $^4I_{13/2}$), and short-living level 3 the higher lying excited states ($^4I_{11/2}$ and the upper Er^{3+} manifolds).

At these assumptions, we imply regarding the subsystem of single Er^{3+} ions that they can occupy under the pump-light action the only two states (1 and 2) through interplay between the GSA, SE, and ESA processes, attributed by cross-sections σ_{12}, σ_{21}, and σ_{23}, respectively, and also by ASE. In addition, the HUC process, attributed by constant $C_{HUP}*$, ought to be applied for single ions; see subsection III.A.

As about Er^{3+} ions forming clusters, we assume that the IUC process has an important difference as compared to the HUC one, namely, it is characterized by such interaction of a cluster's constituents that all they except one leave state 2

(down to state 1) very fast whereas the only excepted one can exist in state 2. Worth noticing, such situation appears only in a pumped fiber and cannot exist at the measurements of SSA, which is the cause of NSA loss in EDFs with high Er^{3+} content. We also assume that a cluster of Er^{3+} ions has only the two states – state <11>, where all ions forming the cluster except one are in the ground state, and state <12>, where this excepted ion (an acceptor of energy transferred from the adjacent donor ions within the cluster) is a sole that is permitted to occupy the excited state. It is postulated that the processes in which clustered ions are involved under the pump action are attributed by the same microscopic parameters that apply for single ions (*i.e.* σ_{12}, σ_{21}, σ_{23}, and τ_0).

Apparently, the HUC process is not applicable to clustered ions and, vice-versa, the IUC process is not applicable to single ones.

The other difference between clustered and single Er^{3+} ions, as it stems from Section II, is the presence of short relaxation time τ_1 (measured by 20…30 μs; see Fig. 7), which relates to Er^{3+} concentration-dependent unsaturated NSA loss (see Figs. 8–10). In accord with the above made definitions for single and clustered species, the short relaxation time ought to apply to rather the latter than to the former species, because the singles solely experience HUC (see above).

The physical origin of the short relaxation time τ_1 is not fully clear to us at the moment but seems to be a process with rate of leaving the first excited state by the constituents of a cluster, excepting one that accepts the energy of other constituents. The excess of energy received by the acceptor is released mostly through UC emissions (see Fig. 2) and / or dissipated via electron-phonon coupling. Thus, time τ_1 seems to be a measure of specific excitation relaxation, more effective for clustered than for single Er^{3+} ions. We take into account the presence of time τ_1 (along with τ_0) for Er^{3+} clusters as an essential element of our model, coming from the experimental data. In the meantime notice that there are other estimates for the characteristic excitation relaxation time in clustered Er^{3+} ions in EDFs, spanned from the lowest limit ~50 ns [46] to μs-range (see *e.g.* Refs. [5], [8], [14], [27], [37]). However, this difference doesn't affect much the results of our modeling (see below) because $\tau_1 << \tau_0$ in any case.

Considering that the population densities of single and clustered Er^{3+} ions in an EDF, $N_{1,2}^{s,c}$, satisfy the following relations:

$$N_1^s + N_2^s = N_0^s = N_0 (1 - \Omega\kappa) \tag{3a}$$

$$N_1^c + N_2^c = N_0^c = \Omega\kappa N_0 \tag{3b}$$

where κ is the partial weight of clustered ions in ensemble, Ω is the effective number of Er^{3+} ions in a cluster, and N_0 is the overall Er^{3+} ions concentration. The correspondent normalized population densities are defined as $n_{1,2}^{s,c} = N_{1,2}^{s,c}/N_0$, where lower indices assign, correspondingly, the ground (1 or <11>) and the first excited (2 or <12>) states, and $N_0^{s,c}$ are the concentrations of single ions and clusters, respectively.

The balance equations for pump power (P) and normalized dimensionless population densities of single and clustered ions being in metastable states 2 and <12>, $n_2^{s,c}$ ($0 \leq \quad n_2^{s,c} \leq 1$), are as follows:

$$\frac{dP}{dz} = -\alpha_0 P \left\{1 - (1 + \xi - \eta)\left(n_2^s + n_2^c\right)\right\} - \gamma_0 P \tag{4}$$

$$\frac{\alpha_0}{h\nu N_0 \Gamma S_a}\left[\Omega\kappa - (1+\xi)\, n_2^c\right]P - \left(\frac{1}{\tau_0} + \frac{1}{\tau_1}\right) n_2^c = 0 \tag{5}$$

$$\frac{\alpha_0}{h\nu N_0 \Gamma S_a}\left[1 - \Omega\kappa - (1+\xi) n_2^s\right]P - \frac{n_2^s}{\tau_0} - C_{HUP}\left(n_2^s\right)^2 = 0 \tag{6}$$

where quantities α_0, τ_0, τ_1, and C_{UP} have been introduced earlier; parameters ξ and η are defined as $\xi = \sigma_{21}/\sigma_{12}$ and $\eta = \sigma_{23}/\sigma_{12}$; Γ is the optical field / fiber core overlap factor at the pump wavelength; γ_0 is the linear (background) loss coefficient; $S_a = \pi r_0^2$ is the EDF core area; $h\nu = hc/\lambda_e$ is the pump energy quanta (h is Planck constant and c is free-space light velocity). In Eqs. (4–6) we omit the ASE contribution as negligible in our experiments at pump powers in excess of 0.5 mW; see section II.

Note that Eqs (4–6) written in a general form are applicable not only to the Er^{3+} ion but also to any other resonantly absorbing center, having a three equivalent level system and subjected to the aforementioned concentration effects. In the meantime, for our experimental arrangement ($P \equiv P_{978}$), these equations are substantially simplified. Indeed, given by a pump wavelength's spectral position ($\lambda_e = 978$ nm) and negligible population of level 3, the SA transition can be disregarded, which ensures zeroing of the ratio $\xi = \sigma_{21}/\sigma_{12}$(we made the same approximation at modeling the EDFs' fluorescence kinetics). Furthermore, neglecting the ESA transition at 978-nm pumping ($\sigma_{23} = 0$) is also a valid approximation, which allows us considering the ratio $\eta = \sigma_{23}/\sigma_{12}$to be null, too.

We calculated output power P^{out} (at 978 nm) as a function of P^{in} for each EDF and found the transmission coefficient as $T_{978} = P^{out}/P^{in}$. The nonlinear absorption coefficient was found accordingly, applying the definition introduced in the experimental part: $\alpha\,(P^{in}) = -ln(T_{978})/L_0$ (remind, L_0 is the length of an EDF sample).

The parameters' values used at modeling are listed in Table 1 in the five left-hand columns; these are the values known or calculated from the fabricants' data or existing literature on silica-based EDFs. The overall concentrations of Er^{3+} ions N_0 (column 6 in Table 1) can be estimated using the relation$N_0 = \alpha_0/\Gamma\sigma_{12}$, where σ_{12}-value at 978 nm was taken to be 1.7×10^{-21} cm^2 (an average value found from the literature on silica-based EDFs; see *e.g.* Refs. [34], [37], [47]–[49]). The other parameters' values used are as follows: $\tau_0 = 10.8$ ms; $\tau_1 = 21$ μs (for the EDFs of L type) and 26 μs (for the EDFs of M type); $C_{HUP}* = 2.7 \times 10^{-18}$s^{-1}cm^3 (see subsection III.A). The linear loss coefficients γ_0 were taken to be the loss measured far away from the Er^{3+} absorption bands (at ~1300 nm): $\gamma_0 = 0.03…0.1$ dB/m (weakly depending upon the EDF type). The only quantities we varied for fitting the experimental dependences $\alpha(P^{in})$ (symbols in Fig. 9) were the coefficients κ (the relative content of Er^{3+} ion clusters) and Ω (the number of Er^{3+} ions in a cluster).

The modeling results are plotted by plain curves 1 to 5 in Fig. 9. It is seen that they fit well the whole of the experimental

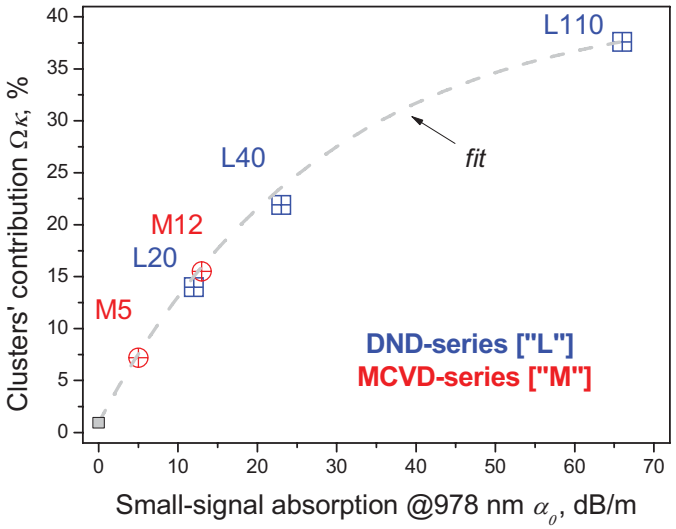

Fig. 12. Er^{3+} clusters' contribution $\Omega\kappa$ *vs.* Er^{3+} concentration (in terms of SSA α_0) obtained for the entire set of EDFs of L and M types as the result of modeling the experimental dependences of nonlinear absorption coefficient using Eqs (4–6); the fitting curve is for guiding the eye.

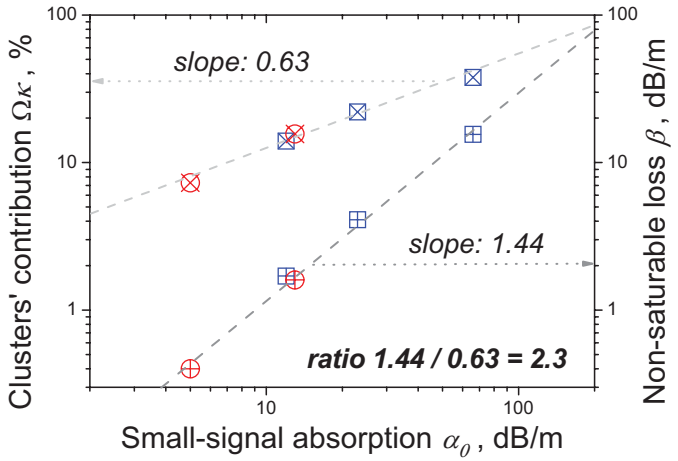

Fig. 13. Er^{3+} clusters' contribution $\Omega\kappa$ (left scale) and non-saturable absorption loss β (right scale) *vs.* Er^{3+} concentration (in terms of SSA α_0) obtained for the entire set of EDFs of L and M types; the ratio of the slopes attributing the dependences reveals an effective number of Er^{3+} ions in clusters.

data for the EDFs of both types. Thus, the IUC process, treated by us as mostly non-radiative relaxation within Er^{3+} ion clusters, is justified as the key mechanism responsible for NSA (attributed by coefficient β, see above). The dependence of coefficient β upon Er^{3+} concentration in terms of SSA α_0 is shown in Fig. 10 (by curve 1) as the result of modeling; the errors' bars in the curve show uncertainties of fitting the experimental data by the theory.

When making the numerical calculations, we found that, once searching for the best fit of the experiment by the theory, any Ω-value ($\Omega = 2,3...m$) can be used, with κ-value being varied accordingly. Thus, we have concluded that the product $\Omega\kappa$ (a relative number of clustered Er^{3+} ions in the system) serves an adjusting parameter at fitting rather than quantities Ω and κ separately; refer as well to Eqs (4–6). Its dependence upon SSA α_0 is demonstrated in Fig. 12 (see also column 8 in Table 1). Notice that, like at the modeling of Er^{3+} fluorescence kinetics (where the HUC process is involved), these data for the EDFs of M and L series form a single curve (shown in Fig. 10 as a fit for guiding the eye). Hence, we can conclude that, regardless the technology used at the EDFs fabrication (MCVD or DND), both inspected UC effects, HUC and IUC, obey very similar Er^{3+} concentration-related trends. In the meantime, emphasize that if the concentration dependence of $\Omega\kappa$ for the EDFs of L type can be extrapolated to the lower α_0–values without big errors, the one for the EDFs of M type – cannot (unfortunately we didn't have in disposal an EDF of M type with higher than 12.5 dB/m small-signal absorption at 978 nm, as non-available at the market).

Given by the modeling results, a useful insight can be made to interrelation between the relative number of clustered Er^{3+} ions $\Omega\kappa$ (modeling: Fig. 12) and the measured NSA value β (experiment: Fig. 10). Building on the same plot (at double logarithmic scaling) the dependences of these two quantities *vs.* the SSA-value α_0, we found that they have the slopes related as ($\sim$1.44/$\sim$0.63) $\approx$ 2.3; see Fig. 13.

Apparently, the found value signifies nothing than the average number of Er^{3+} ions in clusters, whose presence, according to the model, is responsible for NSA. This result deserves attention since it shows that NSA in the EDFs of both types mostly originates from paired Er^{3+} ions rather than from more complicate aggregates. Thus, in contrast to, say, Ref. [14] where it is discussed the role of "heavier" clusters in the IUC phenomenon, our results evidence for negligible contribution of Er^{3+} clusters, "heavier" than simple ion pairs. Worth noticing is that this conclusion could not be made by anyway rather than by means of the modeling, taken into account clustering of an arbitrary number of Er^{3+} ions in a cluster.

The rest of the modeling results are provided in the four right-hand columns of Table 1. Noteworthy is the fact that the interrelation between the estimates for Er^{3+} ions concentration and the percentages of the clustered (mostly paired) Er^{3+} ions in ensemble fairly match the trend found in the earlier studies on the matter; see *e.g.* Refs. [8], [10], [28].

Before to conclude, notice that the presence in EDFs of NSA at increasing Er^{3+} concentration is a drawback: Obviously, net gain in heavily-doped Er^{3+} fibers becomes more and more limited (saturated) as it mainly stems from the presence of single Er^{3+} ions being in the excited state, whereas the clustered ions, in their big part (*i.e.* Ω-1 ions in each cluster) are always in the ground state. As a consequence, efficiency of an EDF-based laser or amplifier is expected to drop with increasing concentrations of Er^{3+} ions in the active fiber. Some recent studies confirm a severe character of the problem [49], [50]. It seems that another problem could be encountered at the use of heavily-doped EDFs for pulsed operation where extensive heating via excitation relaxation within Er^{3+} clusters (being also a NSA-related phenomenon) would affect the dispersive properties of the fibers and deteriorate thereafter the regime.

IV. Conclusion

We analyzed, both experimentally and theoretically, the basic concentration-related phenomena in commercial

Erbium-doped silica fibers (EDFs) fabricated through MCVD (M series) and DND (L series) processes at 978-nm pumping – deviation of fluorescence decay measured at ~1.53 μm from the exponential law ("concentration quenching" via homogeneous upconversion, HUC) and non-saturable absorption (NSA) arising under the pump action due to the presence of clustered Er^{3+} ions in the fibers ("excessive loss" via inhomogeneous upconversion, IUC). The found trends that HUC and IUC obey are shown to be quite similar in fibers of both types. This most probably stems from likelihood of the physical nature of Er^{3+} clustering in the EDFs having similar core-glass chemical composition (alumino-silicate glass) and a minor role of the fabrication technology (MCVD or DND) utilized.

It is demonstrated that the whole of the experimental dependences, featuring the HUC and IUC phenomena, are accurately modeled, employing a simple theoretical model, capable for determining the basic HUC / IUC parameters for the fibers. In particular, for both types of EDFs (L and M) we reveal that the parameter addressing the HUC process is measured to be $C_{HUP}* = 2.7\times10^{-18}$ $s^{-1}cm^3$. Furthermore, the quantity characterizing the IUC process in both types of EDFs, is shown to be the product of the relative content of Er^{3+} ion clusters κ and the number of Er^{3+} ions in a cluster Ω, which monotonously grows with increasing Er^{3+} concentration and approach 37% of overall ions concentration in EDF L110, having small-signal absorption of 67.5 dB/m at 978 nm. The fitting procedure applied to model growth of residual (non-saturable) NSA-loss in the fibers at 978-nm pumping reveals that the average number of ions per a cluster is Ω ~2.3 regardless the EDF type (L or M).

Let's emphasize that the obtained results only relate to the EDFs of L and M series, which are the representatives of the fibers fabricated through the DND and MCVD technologies, mostly known at the fiber market; apparently other EDFs obtained through the MCVD / DND processes can have quite different appearance of the Er^{3+} concentration effect. In the meantime, we believe that the results highlighted in the present study would have impact for future applications of the featured commercial EDFs of L and M types as well as of other EDFs with a similar core-glass type.

REFERENCES

[1] P. Blixt, J. Nilsson, T. Carlinas, and B. Jaskorzynska, "Concentration-dependent upconversion on Er^{3+}-doped fiber amplifiers: Experiments and modeling," *IEEE Trans. Photon. Technol. Lett.*, vol. 3, no. 11, pp. 996–998, Nov. 1991.

[2] E. Delevaque, T. Georges, M. Monerie, P. Lamouler, and J.-F. Bayon, "Modeling of pair-induced quenching in Erbium-doped silicate fibers," *IEEE Photon. Technol. Lett.*, vol. 5, no. 1, pp. 73–75, Jan. 1993.

[3] G. Nikolak, P. C. Becker, J. Shmulovich, Y. H. Wong, D. J. DiGiovanni, and A. J. Bruce, "Concentration-dependent $^4I_{13/2}$ lifetimes in Er^{3+}-doped fibers and Er^{3+}-doped planar waveguides," *IEEE Photon. Technol. Lett.*, vol. 5, no. 9, pp. 1014–1016, Sep. 1993.

[4] J. Nilsson, B. Jaskorzynska, and P. Blixt, "Performance reduction and design modification of Erbium-doped fiber amplifiers resulting from pair-induced quenching," *IEEE Photon. Technol. Lett.*, vol. 5, no. 12, pp. 1427–1429, Dec. 1993.

[5] R. S. Quimby, W. J. Miniscalco, and B. Thompson, "Clustering in Erbium-doped silica glass fibers analyzed using 980 nm excited-state absorption," *J. Appl. Opt.*, vol. 78, no. 8, pp. 4472–4478, Jul. 1994.

[6] F. Di Pasquale and M. Federighi, "Modeling of uniform and pair-induced upconversion mechanisms in high-concentration Erbium-doped silica waveguides," *J. Lightw. Technol.*, vol. 13, no. 9, pp. 1858–1864, Sep. 1995.

[7] J. Nilsson, P. Blixt, B. Jaskorzynska, and J. Babonas, "Evaluation of parasitic upconversion mechanisms in Er^{3+}-doped silica-glass fibers by analysis of fluorescence at 980 nm," *J. Lightw. Technol.*, vol. 13, no. 3, pp. 341–349, Mar. 1995.

[8] E. Maurice, G. Monnom, B. Dussardier, and D. B. Ostrowsky, "Clustering-induced nonsaturable absorption phenomenon in heavily Erbium-doped silica fibers," *Opt. Lett.*, vol. 20, no. 24, pp. 2487–2489, Dec. 1995.

[9] S. Collin, E. Contesse, P. Le Boudec, G. Stephan, and F. Sanchez, "Evidence of a satuarble-absorption effect in heavily Erbium-doped fibers," *Opt. Lett.*, vol. 20, no. 24, pp. 1987–1989, Dec. 1996.

[10] P. Myslinski, D. Nguyen, and L. Chrostowski, "Effects of concentration on the performance of Erbium-doped fiber amplifiers," *J. Lightw. Technol.*, vol. 15, no. 1, pp. 112–119, Jan. 1997.

[11] M. P. Hehlen, N. J. Cockroft, T. R. Gosnell, A. L. Bruce, G. Nikolak, and J. Shmulovich, "Uniform upconversion in high-concentration Er^{3+}-doped soda lime silicate and aluminosilicate glasses," *Opt. Lett.*, vol. 22, no. 11, pp. 772–774, Jun. 1997.

[12] J. L. Philipsen and A. Bjarklev, "Monte Carlo simulation of homogeneous upconversion in Erbium-doped silica glass," *IEEE J. Quantum Electron.*, vol. 33, no. 5, pp. 845–854, May 1997.

[13] B. N. Samson, W. H. Loh, and J. P. de Sandro, "Experimental evidence of differences in the absorption spectra of clustered and isolated ions in Erbium-doped fibers," *Opt. Lett.*, vol. 22, no. 23, pp. 1763–1765, Dec. 1997.

[14] H. L. An, E. Y. B. Pun, H. D. Liu, and X. Z. Lin, "Effects of ion clusters on the performance of heavily doped Erbium-doped fiber laser," *Opt. Lett.*, vol. 23, no. 15, pp. 1197–1199, Aug. 1998.

[15] J. L. Philipsen, J. Broeng, A. Bjarklev, S. Helmfrid, D. Bremberg, B. Jaskorzynska, and B. Palsdottir, "Observation of strongly non-quadratic upconversion in Er^{3+}-doped silica fibres and reevaluation of the degree of clustering," *IEEE J. Quantum Electron.*, vol. 35, no. 11, pp. 1741–1749, Nov. 1999.

[16] B. Srinivasan, R. K. Jain, and G. Monnom, "Indirect measurement of the magnitude if ion clustering at high doping densities in Er:ZBLAN fibers," *J. Opt. Soc. Amer. B*, vol. 17, no. 2, pp. 178–181, Feb. 2000.

[17] F. Vetrone, J.-C. Boyer, J. A. Capobianco, A. Speghini, and M. Bettineli, "980 nm excited upconversion in an Er-doped ZnO–TeO_2 glass," *Appl. Phys. Lett.*, vol. 80, no. 10, pp. 1752–1754, Mar. 2002.

[18] A. Bellemare, "Continuous-wave silica-based Erbium-doped fibre lasers," *Progr. Quantum Electron.*, vol. 27, no. 4, pp. 211–266, Apr. 2003.

[19] E. Yahel and A. A. Hardy, "Modeling and optimization of short Er^{3+}-Yb^{3+} codoped fibre lasers," *IEEE J. Quantum Electron.*, vol. 39, no. 11, pp. 1444–1451, Nov. 2003.

[20] X. Dong, N. Q. Ngo, P. Shum, B.-O. Guan, H.-Y. Tam, and X. Dong, "Concentration-induced nonuniform power in tunable Erbium-doped fiber lasers," *Opt. Lett.*, vol. 29, no. 4, pp. 358–360, Feb. 2004.

[21] A. V. Kir'yanov, Y. O. Barmenkov, and N. N. Il'ichev, "Excited-state absorption and ion pairs as sources of nonlinear losses in heavily doped Erbium silica fiber and Erbium fiber laser," *Opt. Exp.*, vol. 13, no. 21, pp. 8498–8507, Oct. 2005.

[22] A. Y. Plotskii, A. S. Kurkov, M. Y. Yashkov, M. M. Bubnov, M. E. Likhachev, A. A. Sysolyatin, A. N. Gur'yanov, and E. M. Dianov, "Amplifying properties of heavily Erbium-doped active fibers," *Quantum Electron.*, vol. 35, no. 6, pp. 559–562, 2005.

[23] D. Khoptyar, S. Sergeyev, and B. Jaskorzynska, "Homogeneous upconversion in Er-doped fibers under steady state excitation: Analytical model and its Monte Carlo verification," *J. Opt. Soc. Amer. B*, vol. 22, no. 3, pp. 582–590, Mar. 2005.

[24] D. Khoptyar and B. Jaskorzynska, "Experimental determination of the energy-transfer parameters for homogeneous upconversion in Er-doped silica," *J. Opt. Soc. Amer. B*, vol. 22, no. 10, pp. 2091–2098, Oct. 2005.

[25] S. Sergeyev, S. Popov, D. Khoptyar, A. T. Friberg, and D. Flavin, "Statistical model of migration-assisted upconversion in a high-concentration Erbium-doped fiber amplifier," *J. Opt. Soc. Amer. B*, vol. 23, no. 8, pp. 1540–1543, Aug. 2006.

[26] V. Lopez, G. Paez, and M. Strojnik, "Characterization of upconversion coefficient in Erbium-doped materials," *Opt. Lett.*, vol. 31, no. 11, pp. 1660–1662, Jun. 2006.

[27] J. Li, K. Duan, Y. Wang, W. Zhao, Y. Guo, and X. Lin, "Modeling and optimizing of high-concentration Erbium-doped fiber amplifiers with consideration of ion-clusters," *Opt. Commun.*, vol. 277, no. 1, pp. 143–149, Sep. 2007.

[28] B. Dussardier, W. Blanc, and G. Monnom, "Luminiscent ions in silica-based optical fibers," *Fiber Integr. Opt.*, vol. 27, no. 6, pp. 484–504, 2008.

[29] J. Li, K. Duan, Y. Wang, W. Zhao, J. Zhu, Y. Guo, and X. Lin, "Modeling and effects of ion pairs in high-concentration Erbium-doped fiber lasers," *J. Modern Opt.*, vol. 55, no. 23, pp. 447–458, Dec. 2008.

[30] A. Bahrampour, S. Keyvaninia, and M. Karvar, "An inhomogeneous theory for the analysis of an all-optical gain-stabilized multichannel Erbium-doped fiber amplifier in the presence of ion pairs," *Opt. Fiber Technol.*, vol. 14, no. 1, pp. 54–62, Jan. 2008.

[31] O. G. Calderon, S. Melle, F. Arrieta-Yanez, M. A. Anton, and F. Carreno, "Effect of ion pairs in fast-light bandwidth in high-concentration Erbium-doped fibers," *J. Opt. Soc. Amer. B*, vol. 25, no. 12, pp. C55–C60, Dec. 2008.

[32] C. Berkdemir and S. Ozsoy, "On the temperature-dependent gain and noise figure of C-band high-concentration EDFAs with the effect of cooperative upconversion," *J. Lightw. Technol.*, vol. 27, no. 9, pp. 1122–1127, May 2009.

[33] M. Jung, Y. M. Chang, Y. M. Jhon, and J. H. Lee, "Combined effect of pump excited state absorption and pair-induced quenching on the gain and noise figure in bismuth oxide-based Er^{3+}-doped fiber amplifiers," *J. Opt. Soc. Amer. B*, vol. 28, no. 11, pp. 2667–2673, Nov. 2011.

[34] J. A. Valles, V. Bordejo, M. A. Rebolledo, A. Diez, J. A. Sanchez-Marin, and M. V. Andres, "Dynamic characterization of upconversion in highly Er-doped silica photonic crystal fibers," *IEEE J. Quantum Electron.*, vol. 48, no. 8, pp. 1015–1021, Aug. 2012.

[35] R. I. Laming, S. B. Poole, and E. J. Tarbox, "Pump excited–state absorption in Erbium–doped fibers," *Opt. Lett.*, vol. 13, no. 12, pp. 1084–1086, Dec. 1988.

[36] R. Quimby, "Output saturation in a 980-nm pumped Erbium-doped fiber amplifier," *Appl. Opt.*, vol. 30, no. 18, pp. 2546–2552, Jun. 1990.

[37] P. A. Krug, M. G. Sceats, G. R. Atkins, S. C. Guy, and S. B. Poole, "Intermidiate excited-state absorption in Erbium-doped fiber strongly pumped at 980 nm," *Opt. Lett.*, vol. 16, no. 24, pp. 1976–1978, Dec. 1991.

[38] Y. O. Barmenkov, A. V. Kir'yanov, and M. V. Andres, "Resonant and thermal changes in refractive index in a heavily doped Erbium fiber pumped at wavelength 980 nm," *Appl. Phys. Lett.*, vol. 85, no. 13, pp. 2466–2468, Sep. 2004.

[39] M. Bolshtyansky, I. Mandelbaum, and F. Pan, "Signal excited-state absorption in the L-band EDFA: Simulation and measurements," *J. Lightw. Technol.*, vol. 23, no. 9, pp. 2796–2799, Sep. 2005.

[40] A. D. Guzman-Chavez, Y. O. Barmenkov, and A. V. Kir'yanov, "Spectral dependence of the excited-state absorption of Erbium in silica fiber within the 1.48–1.59 μm range," *Appl. Phys. Lett.*, vol. 92, no. 19, pp. 191111-1–191111-3, May 2008.

[41] A. V. Kir'yanov, Y. O. Barmenkov, and A. D. Guzman-Chavez, "Er^{3+} excited-state absorption in an Erbium-doped silica fiber at the wavelengths 1490–1580 and 978 nm," *Laser Phys.*, vol. 18, no. 11, pp. 1251–1256, Nov. 2008.

[42] Y. O. Barmenkov, A. V. Kir'yanov, A. D. Guzman-Chavez, J. L. Cruz, and M. V. Andres, "Excited-state absorption in Erbium-doped silica fiber with simultaneous excitation at 977 and 1631 nm," *J. Appl. Phys.*, vol. 106, no. 8, pp. 083108-1–083108-6, Oct. 2009.

[43] P. G. Kikn and A. Polman, "Exciton–Erbium interactions in Si nanocrystal-doped SiO_2," *J. Appl. Phys.*, vol. 88, no. 4, pp. 1992–1998, Aug. 2000.

[44] P. G. Kik, M. L. Brongersma, and A. Polman, "Strong exciton-Erbium coupling in Si nanocrystal-doped SiO_2," *Appl. Phys. Lett.*, vol. 76, no. 17, pp. 2325–2327, Mar. 2000.

[45] A. V. Kir'yanov, V. V. Dvoyrin, V. M. Mashinsky, Y. O. Barmenkov, and E. M. Dianov, "Nonsaturable absorption in alumino-silicate bismuth-doped fibers," *J. Appl. Phys.*, vol. 109, no. 2, pp. 023113-1–023113-8, Jan. 2011.

[46] P. Myslinski, J. Fraser, and J. Chrostowski, "Nanosecond kinetics of upconversion process in EDF and its effect on EDFA performance," in *Proc. Opt. Amplif. Their Appl.*, Jan. 1995, p. ThE3.

[47] E. Desurvire, "Study of the complex atomic susceptibility of Erbium-doped fiber amplifiers," *J. Lightw. Technol.*, vol. 8, no. 10, pp. 1517–1527, Oct. 1990.

[48] W. Miniscalco, "Erbium-doped glasses for fiber amplifiers at 1500 nm," *J. Lightw. Technol.*, vol. 9, no. 2, pp. 234–250, Feb. 1991.

[49] E.-L. Lim, S. U. Alam, and D. J. Richardson, "High energy in-band pumped Erbium doped fibre amplifiers," *Opt. Exp.*, vol. 20, no. 17, pp. 18803–18818, Aug. 2012.

[50] E.-L. Lim, S. U. Alam, and D. J. Richardson, "Optimizing the pumping configuration for the power scaling of in-band pumped Erbium doped fiber amplifiers," *Opt. Exp.*, vol. 20, no. 13, pp. 13886–13895, Jan. 2012.

Alexander V. Kir'yanov (M'11) received the M.Sc. degree from the M.V. Lomonosov Moscow State University, Moscow, Russia, in 1986, and the Ph.D. degree in optics and laser physics from A.M. Prokhorov General Physics Institute, Russian Academy of Sciences, Moscow, in 1995. He has been with the A.M. Prokhorov General Physics Institute since 1987. Since 1998, he has been a Research Professor with the Centro de Investigaciones en Optica (CIO), Leon, Mexico. He is also a National Researcher (SNI III), a Regular Member of the Mexican Academy of Sciences, and a Senior Member of the Optical Society of America. He has authored or co-authored over 160 scientific papers and held four patents (Mexico, Russia, and USA). His current research interests include solid-state and fiber lasers and nonlinear optics of the solid state and optical fibers.

Yuri O. Barmenkov (M'11) received the Ph.D. degree in radiophysics and electronics from the Leningrad (St. Petersburg) State Technical University, Leningrad, Russia, in 1991. He was an Assistant Professor and then a Senior Lecturer with the Department of Experimental Physics, St. Petersburg State Technical University, Russia, from 1991 to 1996. Since 1996, he has been a Research Professor with the Centro de Investigaciones en Optica, Leon, Guanajuato, Mexico. He is a National Researcher (SNI III), Mexico and a Regular Member of the Mexican Academy of Sciences. He has authored or co-authored over 130 scientific papers and held three patents. His current research interests include single-frequency, CW and Q-switched fiber lasers, fiber optic sensors, and nonlinear fiber optics.

Gabriel Eduardo Sandoval-Romero received the Masters degree in electrical engineering in 1995, and the Ph.D. degree in technical sciences from the Saint Petersburg State University of Telecommunications, St. Petersburg, Russia, in 2001. He is currently with the Optical and Electrical Sensors Group of the Center of Applied Sciences and Technological Development (CCADET), National Autonomous University of Mexico (Universidad Nacional Autónoma de México), Mexico City. He has worked on the development of optical sensors and optical fiber sensors to measure physical magnitude. His current research interests include fiber optic instrumentation and sensing and monitoring physical, chemical, and biological parameters.

Luis Escalante-Zarate is currently pursuing the Ph.D. degree with the Photonics Division, Centro de Investigaciones en Optica, Leon, Guanajuato, Mexico. His current research interests include nonlinear properties of optical fibers and fiber lasers.